Two-dimensional Yb on a Mo(110) surface

A. Stenborg* and E. Bauer
Physikalisches Institut, Technische Universität Clausthal and Sonderforschungsbereich 126 Göttingen-Clausthal, D-3392 Clausthal-Zellerfeld, Federal Republic of Germany
(Received 8 December 1986)

The adsorption of Yb on a Mo(110) surface is studied by Auger electron spectroscopy, work-function-change ($\Delta\phi$) measurements, low-energy electron diffraction, thermal desorption spectroscopy, and energy-loss spectroscopy with the goal to determine the coordination range which can be obtained in a controlled manner. It is found that the number of nearest neighbors may be changed from 0 to 12 by going from a dilute two-dimensional gas to a multilayer, and that in certain coverage ranges the interatomic distances may be varied continuously. This makes such two-dimensional systems ideally suited for the study of the influence of coordination on the electronic structure.

I. INTRODUCTION

The rare-earth metals and their compounds have been a challenge to the solid-state physicist for many years because of their unusual electronic, magnetic, and structural properties. These unusual properties are a consequence of the overlap of the electronic energy levels of the localized $4f$ and the delocalized $5d6s$ states. A particularly interesting phenomenon is the mixed- or intermediate-valence behavior:[1] the valency as measured with various probes is observed to be nonintegral. This behavior is seen in systems containing Ce, Sm, Eu, Tm, and Yb and occurs whenever the energies of the $4f^n(5d6s)^2$ and of the $4f^{n-1}(5d6s)^3$ configurations are sufficiently close so that fluctuations between the two valence states can occur. The energetic proximity of these levels depends upon the number, distance, and nature of the neighbors of the rare-earth ion cores, which can be changed by pressure, temperature, or compound formation and last but not least by changing the dimensionality of the system. This can be achieved by going from the three-dimensional bulk to the two-dimensional surface or to an adsorbed layer. The surface may be considered as a self-adsorbed layer and may be separated from the bulk by varying the depth sampled by a surface-sensitive probe such as photoelectron spectroscopy via its angle and energy dependence. In this manner it has, for example, been concluded that the mixed valency of Sm metal is not due to temporal valence fluctuations but due to spatial valence variations, with trivalent Sm in the volume and divalent Sm in the surface.[2]

A more flexible way to study the influence of number, distance, and nature of neighboring atoms on the electronic structure of rare-earth metals is to use adsorbed layers on single-crystal surfaces of materials with high surface energy and high work function. In the submonolayer range of these layers the density varies continuously or discontinuously, with ordered structures at sufficiently low temperatures.[3] Varying the coverage and temperature, thus, allows one to vary the number and distance of neighbors in pure rare-earth layers. By increasing the coverage beyond one monolayer the transition to the bulk can be performed. In addition, coadsorption in the submonolayer or multilayer range enables one to change the nature of the neighbors systematically.

There have already been many studies of the electronic structure of rare-earth adsorption layers on several single-crystal substrates using various electron-spectroscopic methods. Most of them were concerned with the prototype mixed-valence rare-earth metals Sm and Yb on Al,[4-7] Cu,[8] Ni,[7] Si,[7,9-11] and Ge (Refs. 9 and 12) surfaces. One problem encountered in the preparation of two-dimensional ordered systems is clustering, which is sometimes of thermodynamic origin,[13] and sometimes attributed to the lack of mobility of the adsorbed atoms.[5] Annealing sometimes produces order[5,14] but frequently leads to reaction with the substrate. An optimal substrate must ensure thermodynamic stability of a two-dimensional layer at submonolayer coverage and must be as stable as possible against reaction with the layer at elevated temperature, while at the same time encouraging multilayer formation.[15] Such substrates are the most densely packed surfaces of refractory metals such as the (110) surfaces of W and Mo or the (0001) plane of Re. These materials are of particular interest also for the study of two-dimensional rare-earth compounds because halogens, chalcogens, and other interesting reaction partners of the rare-earth metals such as other metals can be easily coadsorbed without reaction with the substrate.

Adsorption layers on these surfaces usually have rather complicated temperature-dependent structures as evidenced, for example, by the systems Eu, Gd, and Tb on W(110).[16] Therefore a detailed structural characterization is a prerequisite for a meaningful analysis of the electronic structure. Such a characterization, specifically for Yb on Mo(110), is the subject of this paper. The following techniques are used in this endeavor: Auger electron spectroscopy (AES) for characterization of the growth mode, low-energy electron diffraction (LEED)

for structure analysis, work-function-change ($\Delta\phi$) measurements and low-energy electron-loss spectroscopy (ELS) for rough characterization of the spatial electron distribution, and thermal desorption spectroscopy (TDS) for estimation of the bonding of the adsorbed atoms and for relative coverage determination.

II. EXPERIMENTAL PROCEDURE

The experiments were performed in an ultrahigh-vacuum (UHV) system with a base pressure of about 4×10^{-11} Torr. The Mo crystals were initially oriented to within 0.05° of the (110) orientation but distorted somewhat during the experiments and were therefore changed after some time. The distortion reduced the quality of the LEED pattern and caused minor changes in the $\Delta\phi$ data. After thorough cleaning of the highly polished crystals by extended heating in O_2 at 1300–1400 K, no C, O, or S signal was detectable in the AES spectra. CO contamination during the experiments never exceeded an amount corresponding to C-to-Mo 221-eV and O-to-Mo 221-eV AES signal ratios of 1:300. The crystal was heated by Joule heating and its temperature was measured with a W + 5 at.% Re–W + 26 at.% Re thermocouple and an optical pyrometer.

Yb was evaporated after extensive outgasing in well-reproducible doses from $\frac{1}{100}$ to $\frac{1}{5}$ monolayers (ML) from an indirectly heated Ta tube oven. During the experiments the pressure did not rise above 6×10^{-11} Torr. The AES and ELS measurements were made with a cylindrical-mirror analyzer in the derivative mode with modulation amplitudes of 1 V peak to peak for the Mo 221-eV AES peak, 5 V peak to peak for the C and O AES peaks and 0.5 V peak to peak for the ELS spectra. Only the Mo 221-eV peak was monitored during the depositions because the strong overlap of the Yb and Mo low-energy AES spectrum made a separation of the two spectra too complicated. The primary energies were 1500 eV in the AES and 48 eV in the ELS measurements, and normal incidence was used in both cases.

The $\Delta\phi$ measurements were made in the constant-current mode of the electron-beam retarding-field method with a simple magnetically collimated electron gun. An accuracy of ±10 meV can be achieved easily, but reproducibility is somewhat limited by the thermal prehistory of the crystal and by the amount of residual gas coadsorption during long experiments, in particular in combined $\Delta\phi$-LEED, $\Delta\phi$-AES, and $\Delta\phi$-TDS measurements. Nevertheless, the $\Delta\phi$ measurement was the simplest and most reliable method for the correlation of the results obtained with the various methods.

The TDS study was made with an average heating rate of 9 $K\,s^{-1}$ by desorbing into a quadrupole mass spectrometer through an aperture which limited the accepted region on the crystal to its central part in which the temperature gradient was typically less than 5 K at 1100 K. The desorption parameters in the rate equation for desorption $dn/dt=-n\nu\exp(-E/kT)$ (preexponential factor ν and desorption energy E) were derived from the spectra with a revised version of a program[17] which assumes a single desorption state with coverage- (Θ) dependent ν and E values. Due to the complexity of the spectra the resulting $\nu(\Theta)$ and $E(\Theta)$ values have only semiquantitative character, but the coverage values obtained by integrating the spectra are quantitative.

III. RESULTS

Figure 1 shows the Mo 221-eV Auger signal and the work-function change as a function of the deposition time. The Auger signal can be fitted by three linear segments, which suggests the existence of three coverage regions with different shadowing of the Mo substrate by the adsorbed atoms. No monolayer (ML) calibration is possible, however, on the basis of these data. Therefore, $\Delta\phi$ is used for this purpose. It is a general rule that electropositive adsorbates have a local maximum of $\Delta\phi$ at 1 ML due to the atomic smoothness of the full layer. This puts the monolayer ($\Theta_A=1$) at $t=14.0$ min as seen in the $\Delta\phi$ data of Fig. 1. $\Delta\phi$ shows the coverage (Θ) dependence typical for electropositive adsorbates: after an initial linear decrease which is determined by the dipole moment p_0 of the individual atoms ($\Delta\phi=300\times10^{-18}4\pi np$, $\Delta\phi$ in eV, n in atoms/cm^2, p in debye), $\Delta\phi$ passes through a minimum, here at −2.50 eV, rises to the ML maximum, here at −1.72 eV, and decreases afterwards slowly again. The linear $\Delta\phi$ decrease after 1 ML indicates formation of a second ML in the form of islands which are already large at the beginning of the second ML. Three-dimensional island growth or a two-dimensional gas in the second monolayer would be accompanied by a nonlinear $\Delta\phi$ decrease. The formation of a second ML is supported also by the continued linear decrease of the Mo AES signal, which does not even show the typical slope change at 1 ML. This unusual behavior will be discussed elsewhere.

Returning to the $\Delta\phi$ data in Fig. 1, the linear segments indicated between minimum and maximum and

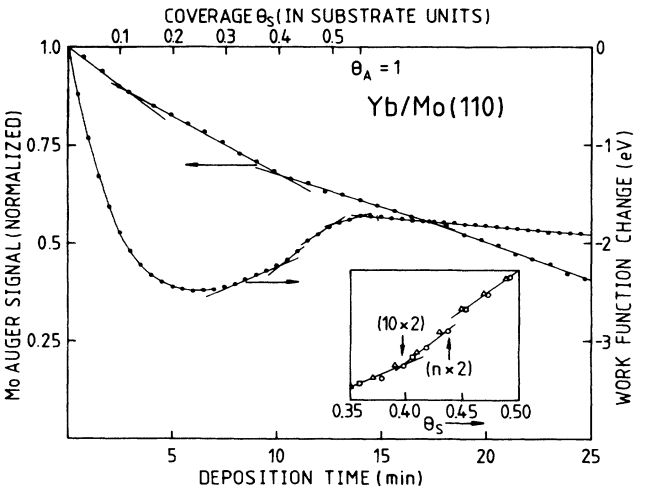

FIG. 1. Mo 221-eV ($M_5N_{4,5}N_{4,5}$) Auger signal and work-function change $\Delta\phi$ as a function of time of deposition of Yb in $\frac{1}{17}$ and $\frac{1}{28}$ monolayer doses, respectively, onto a Mo(110) surface at room temperature. On the top the coverage values Θ_s obtained from combined LEED and $\Delta\phi$ measurements are shown.

the discontinuity at $\Theta_s = 0.43$ have to be justified. They are reproducible whenever the density of points is large enough and are compatible with curves with more widely spaced points (see inset). They coincide with characteristic changes in the LEED patterns (see inset) which will be discussed in detail below. The beginning of the first linear segment at 8 min coincides with the appearance of the 10×2 pattern which changes to an $n\times2$ pattern with Θ-dependent n at the first slope change at 10.1 min. The $\Delta\phi$ discontinuity between 11 and 11.5 min is connected with the transition from the $n\times2$ pattern to a hexagonal pattern with Θ-dependent periodicity. At the last break before the completion of the monolayer the pattern is a coincidence pattern but becomes incommensurate again beyond the break. Therefore the slope changes and the discontinuity are believed to be caused by discontinuous changes of the atomic roughness of the surface connected with the structural changes with increasing coverage.

Some of the LEED patterns and the reciprocal-lattice unit meshes derived from them are shown in Fig. 2. The 10×2 pattern [Figs. 2(a) and 2(b)] which increases from a very weak and diffuse pattern at 8 min to a sharp intense pattern at 10.1 min corresponds to a coverage—referred to the substrate atomic density $n = 14.277\times10^{14}$ cm^{-2}—of $\Theta_s = 0.4$. Figures 2(c) and 2(d) are from the transition region between $n\times2$ and hexagonal pattern at about 11.2 min. n expresses the continuous expansion of the reciprocal unit mesh in the [001] direction with coverage. Finally, Figs. 2(e) and 2(f) show the complex coincidence pattern at 12.6 min. In addition to the strong reflections from the layer—which are *not* located along the major reciprocal-lattice vectors of the substrate—many multiple-scattering points can be seen which allow very precise determination of the adsorbate unit-mesh dimensions relative to those of the substrate. From these the "LEED coverages" shown in Fig. 3 are obtained by assuming that all sites in the adsorbate lattice are occupied. Crosses indicate the 10×2 and $n\times2$ structures, solid circles the hexagonal structure. For the rotated hexagonal structure, the rms deviation from the ideal hexagonal-unit-mesh angle 120° is 0.23° over the whole Θ range, decreases with increasing Θ, and is within the limits of error. The relative coverages agree exceedingly well with the relative deposition times, which is to be expected because the TDS measurements to be discussed below show that the sticking coefficient s is constant, probably $s = 1$, at least up to 1 ML. Above $\Theta_A = 1$ the geometry of the LEED pattern which corresponds to $\Theta_s = 0.55$ does not change any longer so that the LEED and $\Delta\phi$ data are internally consistent. The second AES slope change occurs at the transition from the commensurate 10×2 structure to the incommensurate $n\times2$ structure. This is, therefore, caused by a change in the shielding of the substrate that probably occurs when the completely uncovered substrate areas disappear. The first AES slope change may have the same cause but there are no supporting $\Delta\phi$ or LEED data.

The deduction of the atomic structure of the adsorbate from the reciprocal lattice is a difficult task because it would require an analysis of the intensities of the LEED reflections, which for such complicated patterns is presently beyond the capabilities of the dynamical LEED theory. Therefore structure models have to be discussed which are compatible with the geometry of the LEED pattern and the choice between them has to be based on additional arguments. Figures 4(a)–4(d) show four possible structure models of the 10×2 structure of which (b)–(d) differ only in the position relative to the substrate. Model (a) is based on the frequently invoked high-symmetry site hypothesis in which all atoms are assumed to be in equivalent high-symmetry positions with respect to the substrate. This can be realized by placing all atoms in short bridge positions [Fig. 4(a)], which results in strongly differing nearest-neighbor distances d_0, d_1, d_2 and in the formation of zigzag chains (dashed

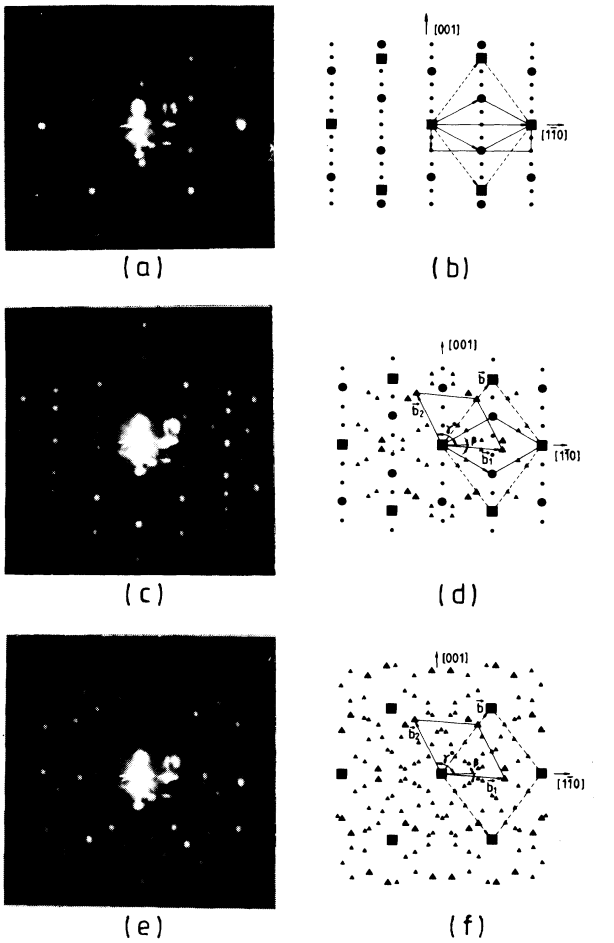

FIG. 2. LEED patterns [(a), (c), (e)] and reciprocal-lattice unit meshes [(b), (d), (f)] of Yb on Mo(110). (a),(b) 10×2 structure ($\Theta_s = 0.4$). (c),(d) Coexisting $n\times2$ (circles) and hexagonal structure (triangles) at $\Theta_s = 0.435$; $b_1 = 0.699b$, $b_2 = 0.700b$, $\gamma^* = 120.05°$, $\beta = 4.81°$. (e),(f) Hexagonal coincidence pattern at $\Theta_s = 0.5$; $b_1 = 0.737b$, $b_2 = 0.738b$, $\gamma^* = 120.05°$, $\beta = 4.81°$. Energies of LEED patterns: 79, 104, and 79 eV, respectively. Squares: Mo reflections; large circles and triangles: Yb reflections; small circles and triangles: double scattering reflections.

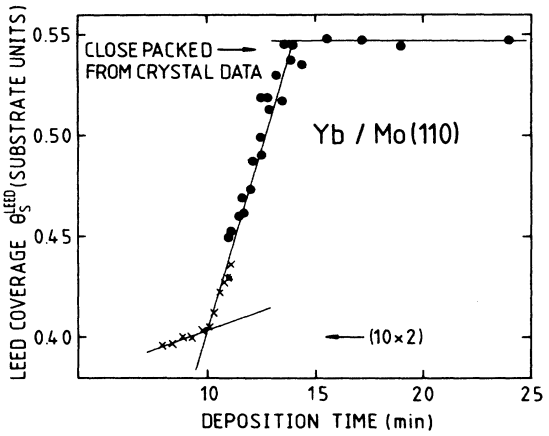

FIG. 3. Coverage as deduced from the LEED pattern as a function of deposition time. Crosses: $n\times 2$ structure; solid circles: hexagonal structure.

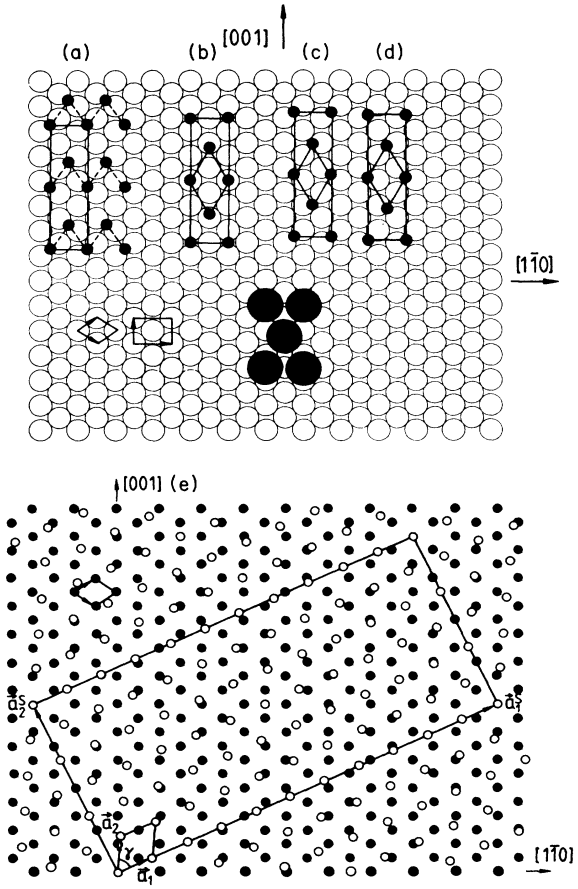

FIG. 4. Models of the 10×2 structure [(a)–(d)] and of the hexagonal coincidence structure (e). For explanation see text. One-half of the 10×2 unit mesh is shown with the correct relative sizes of Yb and Mo atoms. In (e) substrate atoms are indicated by solid circles, adsorbate atoms by open circles, neglecting local displacements.

lines) along the [1$\bar{1}$0] direction. Chain formation along [1$\bar{1}$0] is often observed in adsorption on bcc(110) surfaces and zigzag chains have been invoked repeatedly. However, spot patterns from structures consisting of ordered chains are usually preceded at lower coverages by patterns streaked normal to the chains, which is caused by varying chain spacings. This is not observed here. Furthermore, the distance $d_1=3.855$ Å is smaller than the atomic diameter $d_{Yb}=3.88$ Å, which would require a particularly strong attraction in this direction. Finally, it is difficult to reconcile the symmetry of the most intense adsorbate reflections with the low symmetry of model (a). Therefore the high-symmetry *site* model is considered to be much less likely than the high-symmetry adsorbate models (b)–(d) which produce the strong adsorbate reflections in Figs. 2(a) and 2(b). In these models $d_1=d_2=1.436a=4.52$ Å versus $d_0=\sqrt{2}a=4.45$ Å, i.e., the nearest-neighbor distances differ by only 1.6%. With a unit-mesh angle of $\gamma=121.0°$ the structure is thus close to hexagonal, which is favored in the presence of at least partially repulsive interactions. Of the three relative locations with respect to the substrate which are shown in Figs. 4(b)–4(d), the first one has the largest atomic roughness, the last one, in which all atoms are in equivalent but low-symmetry sites, has the smallest. Model (c) is similarly smooth. On the basis of the work-function increase with increasing perfection and coverage of the 10×2 structure the last two models are slightly favored.

With increasing coverage the layer is compressed continuously in the [001] direction up to a maximum coverage of $\Theta_s=0.438$ at which $d_1=d_2=4.226$ Å and $\gamma=116.4°$. At higher coverages this structure is completely replaced by a rotated hexagonal structure which requires also compression in the [1$\bar{1}$0] direction and which appears first at $\Theta_s\approx 0.43$. The coexistence range of the two structures is small, however (see Fig. 3). For the special case of the coincidence lattice at 12.7 min ($\Theta_s=0.5$), the structure model of Fig. 4(e) results. It has a coverage Θ_s of exactly 0.5 and unit-mesh vectors $\mathbf{a}_1=\frac{3}{11}(3,-3,2)$, $\mathbf{a}_2=\frac{1}{66}(5,-5,84)$, whose lengths differ by 0.15% and which enclose an angle of 59.95°. In addition to the point coincidences seen in Fig. 4(e) there is line coincidence in every second row of adsorbate and substrate atoms parallel to the [$\bar{1}$13] direction. There is another equivalent domain with the rows parallel to [1$\bar{1}$3]. The hexagonal structures at lower and higher coverages are obtained from that in Fig. 4(e) within the limits of error by homogeneous expansion and compression, respectively. At saturation ($\Theta_s=0.547$) the interatomic distance in the hexagonal packing is 3.845 Å, which is 0.9% less than in the bulk, i.e., the monolayer is compressed only very slightly compared to the (111) plane in bulk Yb.

The changes in the bonding between adsorbed atoms and to the substrate with coverage can be deduced from TDS spectra. Figure 5(a) shows a series of TDS spectra in the coverage range $0.01\lesssim\Theta_s\lesssim 0.40$. With increasing coverage a desorption peak shifts initially rapidly from about 1050 K to lower temperatures until an unresolved

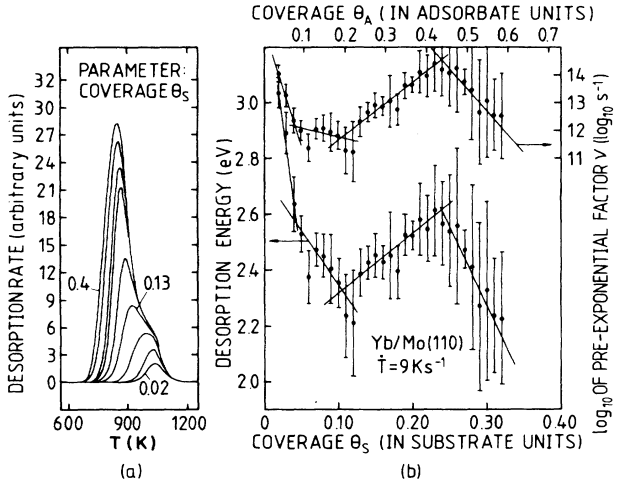

FIG. 5. TDS spectra (a) and desorption parameters (E,ν) derived from them (b) in the coverage range $\Theta_s < 0.4$. The straight lines are drawn to guide the eye.

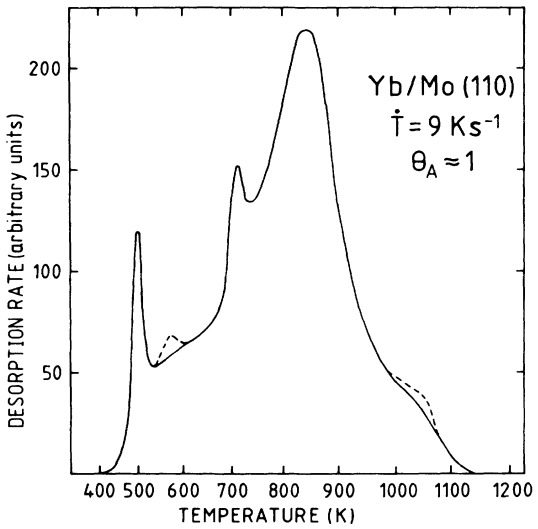

FIG. 6. TDS spectrum from Yb on Mo(110) at a coverage of about one monolayer. Heating rate 9 K s^{-1}.

second peak develops on its low-temperature side. The growth of this peak is connected with a much smaller peak shift. In the analysis of these spectra with an improved version of the method described in Ref. 17 it is assumed that the shape changes of the spectra are caused by the coverage dependence of the desorption parameters E and ν, and not by simultaneous desorption from two different desorption states. The results of the analysis are shown in Fig. 5(b). In spite of the strong scatter and large error bars a decrease of $E(\Theta)$ from $E(0) > 3.0$ eV at $\Theta \to 0$ to about 2.3 eV at $\Theta_s \approx 0.11$ is seen. At larger coverages $E(\Theta)$ initially increases to about 2.6 eV at the work-function minimum ($\Theta_s \approx 0.24$) and then rapidly decreases to about 2.0 eV at $\Theta_s = 0.36$, the highest coverage evaluated. A parallel coverage dependence is seen in ν.

Above $\Theta_s = 0.4$, i.e., when the compression of the 10×2 structure starts, a second binding site is clearly recognizable as a sharp peak on the low-temperature side of the peak seen in Fig. 5(a). Because of the invalidity of the assumption of a single desorption site, no TDS analysis was made at these coverages. The sharp peak is connected with the presence of an incommensurate layer and probably is due to atoms in particularly unfavorable binding sites such as in on-top positions. The spectrum shown in Fig. 6 is from a layer of about 1 ML. The sharp peak at the beginning of the spectrum is from atoms in the second ML, the remaining part is due to the first layer. Also shown is the influence of slight contamination (dashed lines) which was present when the pressure rose into the high 10^{-11}-Torr range during the experiments. It caused characteristic deviations in the low- and high-coverage ranges, which are sensitive indicators of the cleanness of the experiment.

ELS is generally used as an indicator of the electronic structure of the adsorbate, which in turn is connected with its atomic structure. Yb was used in this study because its $4f$ shell is filled so that the complication in the low-energy-loss spectra observed in rare-earth metals with unfilled $4f$ shells[18] should not occur. The loss spectrum from a thick Yb layer [Fig. 7(a)] confirms this: only two pronounced features are seen in the low-loss region, the volume-plasmon loss at $\Delta E = 9.5$ eV and a loss at 4.3 eV which has been attributed alternately to the surface-plasmon loss[19] or to an interband transition,[20] a question which will be dealt with elsewhere.[21] The loss spectrum of the adsorbate is superimposed on that of the substrate [Fig. 7(b)], which consists of three well-pronounced losses: 2.1, 5.2, and 10.6 eV. Three typical spectra, one [Fig. 7(c)] just before the onset of the 10×2 structure, another [Fig. 7(d)] at 1 ML, and the third one [Fig. 7(e)] at 2 ML, illustrate the evolution of the spectrum with coverage. A semiquantitative separation of adsorbate and substrate spectra is possible by following the evolution of the spectra with coverage. In the region below $\Delta E \approx 8$ eV a loss develops initially which overlaps the 2- and 5.2-eV Mo peaks and suppresses them. Its energy can first be determined at $\Theta_A \approx 0.2$ ($\Delta E = 3.0$ eV), from where it rises slowly to 3.1 eV at $\Theta_A \approx 0.5$. Upon condensation into the 10×2 structure, ΔE shifts from 3.4 eV at the beginning of condensation to 3.6 eV at 1 ML ($\Theta_A = 1$). Even at 2 ML ΔE is still far below the value for thick films (3.9 versus 4.3 eV). In the region $\Delta E > 8$ eV, ΔE increases slightly from 9.5 to 9.7 eV at $\Theta_A \simeq 0.5$, then decreases to 9.4 eV at 1 ML and 9.2 eV at 2 ML. The signal (peak-to-peak heights) variations of the low-energy (3.0–4.3 eV) peak and of the peak at ≈ 9.5 eV accompanying these energy changes are illustrated in Fig. 7(f). The signals have been normalized with the signal of the elastically backscattered electrons because inelastic scattering can be seen in the backward direction only when preceded or followed by elastic scattering due to the small angular deflection in inelastic scattering.

The rapid growth of the low-energy loss at small Θ, its ΔE value, and its decrease in the two-dimensional con-

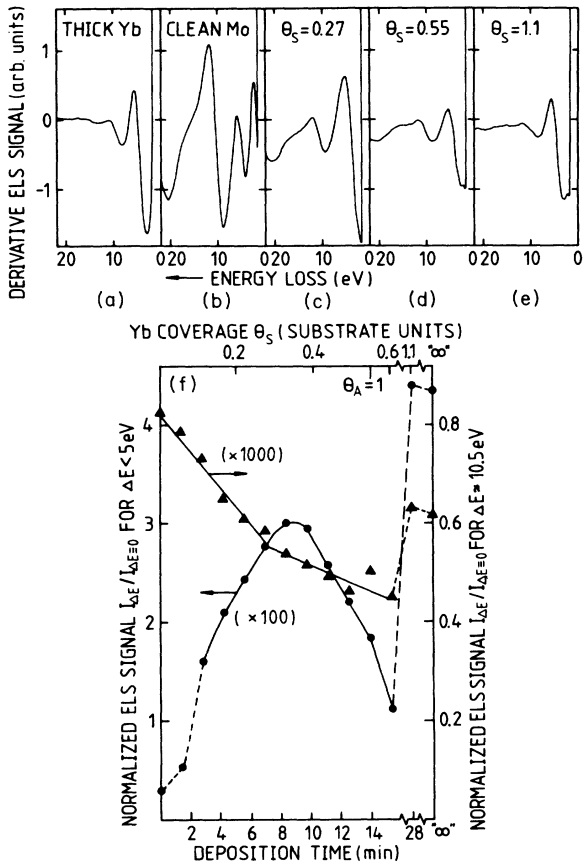

FIG. 7. ELS spectra [(a)–(e)] and ELS signals as a function of coverage of Yb on Mo(110) (f). (a) Thick Yb layer, (b) clean Mo(110), (c) just before condensation into 10×2 structure, (d) at about 1 ML, (e) at 2 ML (in adsorbate units).

densate exclude an interpretation in terms of a surface plasmon or an interband transition. However, it can be easily interpreted by electronic transitions in the atoms of the two-dimensional Yb gas, whose sharp energy levels in free space are broadened and shifted by the interaction with the substrate. The resonance transitions $4f^{14}6s^2 \rightarrow 4f^{14}6s5d$ of Yb and $4f^{14}6s \rightarrow 4f^{14}5d$ of Yb^+ have energies of 3.12 and 3.36 eV, respectively, in the atomic state.[22] The low-coverage loss value of about 3.0 eV suggests, therefore, a resonance excitation of Yb. On the other hand, a strong loss peak at 3.4 eV, which has been assigned to a $4f$-electron excitation, has been observed in atomic Yb.[23] A reliable assignment of the 3.0-eV loss is thus not possible at present. Upon condensation of the two-dimensional gas into a two-dimensional crystal (10×2 structure) the energy levels broaden further into a two-dimensional band structure. As a consequence, the sharp density-of-states features of the valence electrons necessary for peaks in the derivative loss spectra disappear, which causes the decrease of the loss signal. When the third dimension comes into play, a sharpening can occur again due to the increased $\Delta\mathbf{k}\approx 0$ selectivity, causing the observed increase in the derivative loss signal, but surface-plasmon creation cannot be excluded either. In any case derivative ELS appears to be a good monitor of the gas-solid transition in two dimensions.

IV. DISCUSSION

The analysis of the AES, $\Delta\phi$, LEED, TDS, and ELS data, which was presented together with the data themselves in Sec. III, gives a rather detailed picture of the state of Yb adsorbed on Mo(110) at room temperature. At low coverages up to $\Theta_s \approx 0.25$ or $\Theta_A \approx 0.45$, Yb forms a two-dimensional gas with strong repulsive interactions due to dipole-dipole repulsion. Because of the large initial dipole moment $p_0 = \lim_{n\rightarrow 0}(\Delta\phi/n)10^{18}/(300\times 4\pi) = 4.4$ debye, the initial decrease of the desorption energy with Θ is large due to the repulsion between the dipoles upon their increasing density. At about $\Theta_s = 0.04$ this effect decreases not only because of increasing depolarization but probably mainly because of the increasing effect of attractive indirect electronic interactions along the $[1\bar{1}0]$ direction. These have been invoked repeatedly to explain the tendency for the formation of atomic rows along this direction on bcc (110) and (112) surfaces, even at low coverages when the rows are still far apart.[24] Also in the system Yb/Mo(110), ordered structures with row spacings larger than in the 10×2 structure [Figs. 4(b)–4(d)] should occur at lower temperatures because of the local maximum of the binding energy at $\Theta_s \approx 0.24$.

At room temperature the first $[1\bar{1}0]$ row structure, the 10×2 structure, appears in the form of islands—as indicated by weak diffuse reflections—at $\Theta_s \approx 0.3$, which grow until the surface is completely covered with this structure at $\Theta_s = 0.4$. The formation of islands is possible only if the repulsive nearest-neighbor interaction normal to the $[1\bar{1}0]$ rows is overcompensated by an attractive interaction between more distant rows. Inasmuch as it has been shown that zigzag row formation is unlikely, the atomic distribution in the layer is governed by nearest-neighbor repulsion—which favors a hexagonal structure—and by the periodicity imposed by the substrate on the $[1\bar{1}0]$ rows—which favors an $n\times 2$ structure. With increasing coverage the repulsion becomes dominating. This follows from the observation that the $n\times 2$ structure terminates when the distance between nearest atoms in neighboring rows is still significantly larger ($d_1 = d_2 = 4.23$ Å) than the atomic diameter of Yb (3.88 Å). Only hexagonal layers, rotated with respect to the substrate, are, therefore, seen in the high-coverage range of the first layer. The absence of strong compression in the saturated monolayer is probably the cause that a second layer and probably more layers are formed on top of it instead of three-dimensional crystals, possibly in a metastable manner ("pseudo–Frank–van der Merwe growth"[25]).

There are very few Yb adsorption data on single-crystal surfaces for comparison. On Al(100) a $(\sqrt{5}\times\sqrt{5})R27°$ LEED pattern was observed upon deposition of 3 Å of Yb (Ref. 4) but no more detail is given. On Ni(110) a 2×1 structure is obtained after annealing resulting in considerable interdiffusion[7] and on Si(111)

several structures are formed which were also characterized by ion scattering spectroscopy.[7,14] After annealing about 1 ML at increasingly higher temperatures and associated decreasing coverage due to interdiffusion, 2×1, 5×1, and 3×1 structures were found.[7,14] For all other Yb-on-substrate systems no structural characterization is available, so the electron spectroscopic information could be compared only with the layer thickness, which was usually in the mono- to multilayer range.

A comparison which is more important for future electron spectroscopic work on rare-earth metals on metal surfaces is the comparison with other rare-earth metals on Mo and W (110) surfaces. Of particular interest here are mixed-valence adsorbates of which only Eu on W(110) and Sm on Mo(110) have been characterized structurally up to now.[16,21] Eu is also divalent as Yb is and has a half-filled $4f$ shell. Its atomic diameter is somewhat larger than that of Yb, 4.08 versus 3.88 Å, and this may be one reason for the structural differences: order in the form of a 3×2 pattern ($\Theta_s=\frac{1}{3}$) begins already at $\Theta_s\approx0.26$ at room temperature and an unrotated hexagonal pattern appears already at $\Theta_s=0.3$. Also at higher coverages, Eu and Yb differ significantly. For more details see Ref. 16. Summarizing the situation of the rare-earth metals on bcc (110) surfaces it can be said that the qualitative features are sometimes similar (e.g., Tb versus Gd) but all systems seem to differ at least quantitatively. Some general rules are apparent at present, for example the $[1\bar{1}0]$ row formation at low coverages, but much work still needs to be done to understand these rules and others to be found.

V. SUMMARY

The study presented here lays the structural foundation for a systematic study of the influence of dimensionality on the electronic structure of rare-earth metals. This was achieved for the specific example of the mixed-valence candidate Yb on Mo(110) by combining AES, $\Delta\phi$, LEED, TDS, and ELS measurements to develop models of the structure of the adsorbate as a function of coverage. The results show that Yb can be produced as a two-dimensional gas of individual atoms with selectable density, as an array of one-dimensional systems whose distance probably can be varied by cooling, as a two-dimensional condensate with adjustable density, and as a multilayer system at least as a metastable one. In this manner it is possible to study the influence of dimensionality D on the electronic structure from $D=0$ to $D=3$, from 0 to 12 nearest neighbors and in $D=0,2$, possibly also in $D=1$ as a function of distance. Thus it is not necessary any longer to rely on roughness effects,[26] which are difficult to control. Intermixing with the substrate as it occurs upon annealing in order to establish order on the surfaces studied to date (Al, Ni, Si, Ge) does not occur in the submonolayer range on W and Mo (110) surfaces. Furthermore, preadsorption, coadsorption, or postadsorption of other adsorbates—many of which have been studied by themselves on these surfaces—allows a controlled change of the chemistry far beyond what is possible in three dimensions because the composition can be varied at will. One drawback of electron spectroscopic studies on two-dimensional systems on W and Mo (110) carriers is the requirement of extreme cleanness which, however, is increasingly achieved with present-day spectrometers.

ACKNOWLEDGMENT

One of us (A.S.) wants to acknowledge support by The Swedish Institute.

*Permanent address: Uppsala Universitet, Department of Physics, Box 530, S-751 21 Uppsala, Sweden.

[1]For an overview see J. M. Lawrence, P. S. Riseborough, and R. D. Parks, Rep. Prog. Phys. **44**, 1 (1981); *Valance Instabilities,* edited by P. Wachter and H. Boppart (North-Holland, Amsterdam, 1982).

[2]G. K. Wertheim and G. Crecelius, Phys. Rev. Lett. **40**, 813 (1978); J. K. Lang and Y. Baer, Solid State Commun. **31**, 945 (1979).

[3]For reviews see E. Bauer, in *Interfacial Aspects of Phase Transformations,* edited by B. Mutaftschiev (Reidel, Dordrecht, 1982), p. 411; in *The Chemical Physics of Solid Surfaces and Heterogeneous Catalysis,* edited by D. A. King and D. P. Woodruff (Elsevier, Amsterdam, 1984), Vol. 3B, p. 1

[4]G. G. Tibbetts and W. F. Egelhoff, Jr., J. Vac. Sci. Technol. **17**, 458 (1980).

[5]Å. Fäldt and H. P. Myers, Phys. Rev. B **30**, 5481 (1984); and unpublished.

[6]J. Onsgaard, I. Chorkendorff, O. Ellegaard, and O. Sørensen, Surf. Sci. **138**, 148 (1984).

[7]I. Chorkendorff, J. Kofoed, and J. Onsgaard, Surf. Sci. **152/153**, 749 (1985).

[8]Å. Fäldt and H. P. Myers, Phys. Rev. Lett. **52**, 1315 (1984).

[9]A. Franciosi, P. Perfetti, A. D. Katnani, J. H. Weaver, and G. Margaritondo, Phys. Rev. B **29**, 5611 (1984).

[10]Å. Fäldt and H. P. Myers, Phys. Rev. B **33**, 1424 (1986).

[11]G. Rossi, D. Chandesris, P. Roubin, and J. Lecante, Phys. Rev. B **33**, 2926 (1986).

[12]J. Nogami, C. Carbone, D. J. Friedman, and I. Lindau, Phys. Rev. B **33**, 864 (1986).

[13]A. Fujimori, M. Grioni, and J. H. Weaver, Phys. Rev. B **33**, 726 (1986).

[14]J. Kofoed, I. Chorkendorff, and J. Onsgaard, Solid State Commun. **52**, 283 (1984).

[15]E. Bauer, Appl. Surf. Sci. **11/12**, 479 (1982).

[16]J. Kołaczkiewicz and E. Bauer, Surf. Sci. **175**, 487 (1986).

[17]E. Bauer, F. Bonczek, H. Poppa, and G. Todd, Surf. Sci. **53**, 87 (1975).

[18]J. Kołaczkiewicz and E. Bauer, Phys. Status Solidi B **131**, 699 (1985); unpublished data.

[19]W. D. Schneider, C. Laubschat, G. Kaindl, B. Reihl, and N. Mårtensson, in *Valance Instabilities,* edited by P. Wachter

and H. Boppart (North-Holland, Amsterdam, 1982), p. 277.
[20]J. Onsgaard and Ib Chorkendorff, Phys. Rev. B **33**, 3503 (1986), and references therein.
[21]A. Stenborg and E. Bauer, Surf. Sci. **185**, 394 (1987); and unpublished.
[22]*Gmelin Handbuch der Anorganischen Chemie,* edited by G. Kirschstein (Springer, Berlin, 1976), Vol. 39 B 4, p. 308.
[23]Ib Chorkendorff, J. Onsgaard, H. Aksela, and S. Aksela, Phys. Rev. B **27**, 945 (1983).
[24]For references see Refs. 3 and 16; J. Kołaczkiewicz and E. Bauer, Surf. Sci. **154**, 357 (1985).
[25]E. Bauer and J. H. van der Merwe, Phys. Rev. B **33**, 3657 (1986).
[26]W.-D. Schneider, C. Laubschat, and B. Reihl, Phys. Rev. B **27**, 6538 (1983).

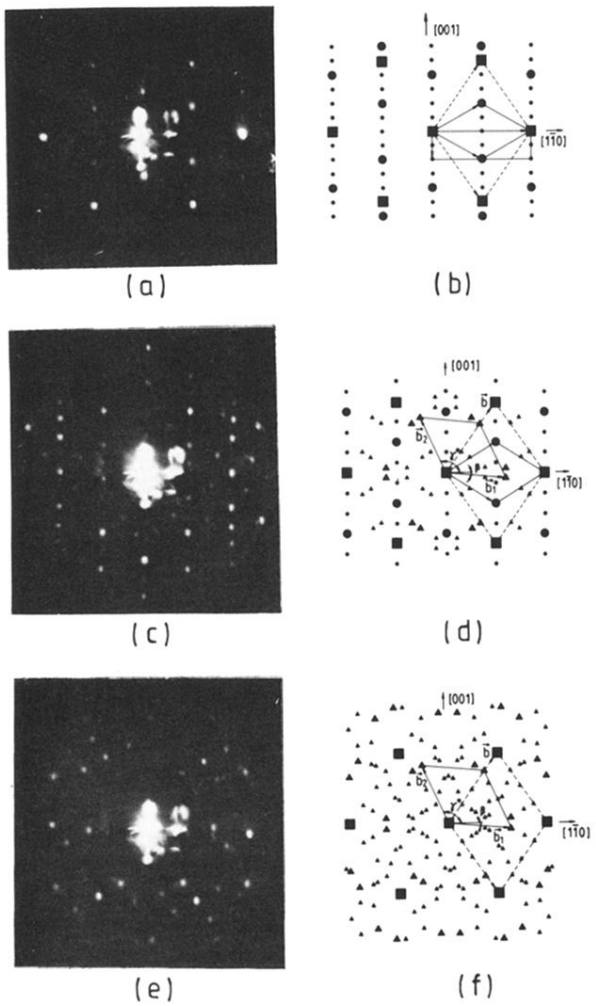

FIG. 2. LEED patterns [(a), (c), (e)] and reciprocal-lattice unit meshes [(b), (d), (f)] of Yb on Mo(110). (a),(b) 10×2 structure ($\Theta_s=0.4$). (c),(d) Coexisting $n\times2$ (circles) and hexagonal structure (triangles) at $\Theta_s=0.435$; $b_1=0.699b$, $b_2=0.700b$, $\gamma^*=120.05°$, $\beta=4.81°$. (e),(f) Hexagonal coincidence pattern at $\Theta_s=0.5$; $b_1=0.737b$, $b_2=0.738b$, $\gamma^*=120.05°$, $\beta=4.81°$. Energies of LEED patterns: 79, 104, and 79 eV, respectively. Squares: Mo reflections; large circles and triangles: Yb reflections; small circles and triangles: double scattering reflections.